J Mol Model (2012) 18:3489–3499
DOI 10.1007/s00894-012-1361-z

ORIGINAL PAPER

Theoretical studies on the Mo-catalyzed asymmetric intramolecular Pauson-Khand-type [2+2+1] cycloadditions of 3-allyloxy-1-propynylphosphonates

Qingxi Meng · Ming Li

Received: 7 September 2011 / Accepted: 10 January 2012 / Published online: 2 February 2012

Abstract Density functional theory (DFT) was used to investigate the Mo-catalyzed intramolecular Pauson-Khand reaction of 3-allyloxy-1-propynylphosphonates. All intermediates and transition states were optimized completely at the B3LYP/6-31 G(d,p) level [LANL2DZ(f) for Mo]. In the Mo-catalyzed intramolecular Pauson-Khand reaction, the C–C oxidative cyclization reaction was the chirality-determining step, and the reductive elimination reaction was the rate-determining step. The carbonyl insertion reaction into the Mo–C(sp^3) bond was easier than into the Mo–C=C bond. And the dominant product predicted theoretically was of (*S*)-chirality, which agreed with experimental data. This reaction was solvent dependent, and toluene was the best among the three solvents toluene, CH_3CN, and THF.

Keywords $Mo(CO)_6$ · Pauson-Khand reaction · Propynylphosphonate · Reaction mechanism · DFT

Introduction

The Pauson-Khand reaction (PKR), formally a [2+2+1] cycloaddition reaction between an alkene, an alkyne, and carbon monoxide to form a cyclopentenone, was first discovered in the 1970s [1–4]. The PKR is a powerful synthetic tool giving a significant upgrade of molecular complexity in a single step. Many transition metals, such as Ti, Fe, Co, Ni, Zr, Ru, Rh, Pd, Ir, and Mo, have been found to be able to catalyze this reaction [5–17]. In addition, the PKR is compatible with many functional groups and enables the construction of relatively complex fused bicyclic structures [6–10]. Vinylphosphonates are important organic intermediates [18–20], and they also possess considerable pharmacological activity [21–23]. Vinylphosphonates produced using octacarbonyldicobalt as a catalyst were reported to undergo an intramolecular PKR to give selective formation of exocyclic 1,3-dienes versus Pauson-Khand cyclopentenone products [24]. Recently, Srebnik and co-workers [25] reported the Mo-catalyzed intramolecular PKR of propynylphosphonates (Scheme 1), and suggested a likely mechanism (Scheme 2) that suggested that the reaction proceeded by the initial complexation to the triple bond [8, 9, 25]. The complexation of the initially formed alkynyl complex with a C–C double bond then results in a Mo-alkynyl-alkenyl complex **B** (Scheme 2). Hence, the Mo-alkynyl-alkenyl complex **B** plays an important role in the $Mo(CO)_6$-catalyzed intramolecular PKR of propynylphosphonates. Srebnik et al. [25] also proved that the reaction was solvent dependent and that the dominant product was of (S)-chirality.

Computational studies on the PKR were performed for the alternative catalysts based on iron [26], cobalt [27], ruthenium [28], and rhodium [29, 30]. Imhof et al. [26] studied the mechanism of the $Fe_2(CO)_9$-catalyzed [2+2+1] cycloaddition reaction between diazabutadiene, carbon monoxide and ethylene at the B3LYP/6-311++G(d,p) level. The calculations indicated that the starting point of the catalytic cycle was the [(diazabutadiene)$Fe(CO)_3$] complex of square-pyramidal geometry. However, Gimbert et al. [31]

Electronic supplementary material The online version of this article (doi:10.1007/s00894-012-1361-z) contains supplementary material, which is available to authorized users.

Q. Meng · M. Li (✉)
College of Chemistry and Chemical Engineering,
Southwest University,
Chongqing 400715, People's Republic of China
e-mail: liming@swu.edu.cn

Q. Meng
College of Chemistry and Material Science,
Shandong Agricultural University,
Taian, Shandong 271018, People's Republic of China

Scheme 1 The Mo-catalyzed intramolecular Pauson-Khand reaction (PKR) of substituted diethyl 3-allyloxy-1-propynylphosphonates

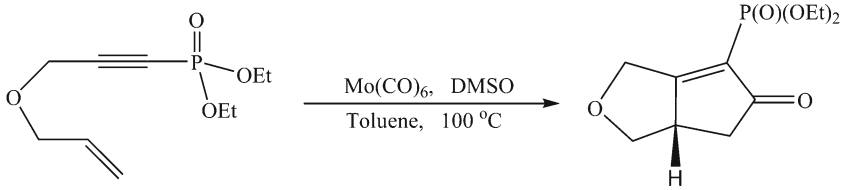

found using electrospray ionization coupled to tandem mass spectrometry that the loss of CO from the PK complex preceded alkene coordination and insertion. Pericàs et al. [27] studied the $Co_2(CO)_6$-catalyzed enantioselective PKR of brucine N-oxide (BNO) at the M06/6-31 G(d) level (LANL2DZ for Co), and proved that this reaction was solvent-dependent. Wang and Wu [28] studied the mechanism of the $Ru_3(CO)_{12}$-catalyzed Pauson-Khand-type [2+2+1] and related [2+2+1+1] cycloadditions at the BP86/6-31 G(d) level (SDD for Ru), and found that insertion into the Ru–C(O) bond was easier than into the Ru–C=C bond. Baik et al. [29, 30] studied the rhodium(I)-catalyzed [2+2+1] carbocyclization reaction of dienes and CO at the B3LYP/6-31 G(d,p) level (LACVP for Rh). They discovered that the addition and removal of CO to control the electron density at the metal center was crucial to facilitating the oxidative addition to form the metallocycle and the reductive elimination to liberate the final product cyclopentenone.

In order to understand the reaction mechanism of the Mo-catalyzed PKR of propynylphosphonates in detail, the Mo(0)-catalyzed intramolecular PKR of substituted dimethyl 3-allyloxy-1-propynylphosphonates was studied in the present work. Specifically, the present study focused on: (1) the energetics of the overall catalytic pathway in the intramolecular PKR; (2) the structural features of intermediates and transition states; (3) the formation of the chiral product; (4) the two pathways of carbonyl insertion; and (5) the effect of the solvent (toluene, CH_3CN, and THF) on the reaction mechanism.

Computational details

All calculations were carried out with the Gaussian 03 program package [32]. The geometries of all species were fully optimized using density functional theory (DFT) [33] using B3LYP method [34, 35] with the 6-31 G(d,p) basis set for all atoms except molybdenum, which was described by the LANL2DZ [36–38] adding one set of *f*-polarization function with an exponent of 1.043 [39]. Frequency calculations were performed to confirm each stationary point to be either a minimum (**M**) or a transition (**T**) structure. The transition states were verified by intrinsic reaction coordinate (IRC) [40] calculations, and by animating the negative eigenvector coordinates with a visualization program (Molekel 4.3) [41, 42]. In addition, bonding characteristics were analyzed by natural bond orbital (NBO) theory [43–46]. NBO analysis was performed by utilizing NBO5.0 code [47]. Furthermore, based on the gas phase optimized geometry for each species, the solvent effects of toluene, CH_3CN, and THF were studied by applying a self-consistent reaction field (SCRF) [48, 49] using the polarizable continuum model (PCM) [50] approach at the same computational level.

Molecular orbital compositions and the overlap populations were calculated with the AOMix program [51, 52]. The analysis of MO compositions in term of occupied and unoccupied fragment molecular orbitals (OFOs and UFOs, respectively), charge decomposition analysis (CDA), and the construction of orbital interaction diagrams were performed using AOMix-CDA [53]. In addition, the electron densities, ρ, at the bond critical points (BCPs) or ring critical

Scheme 2 Proposed mechanism of the Mo-catalyzed intramolecular PKR of substituted diethyl 3-allyloxy-1-propynylphosphonates

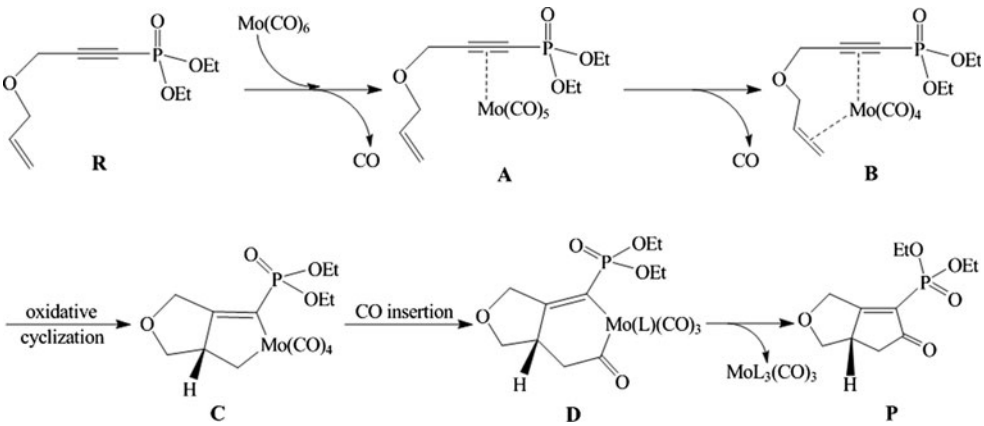

points (RCPs) for some species were calculated with the AIM 2000 program package [54, 55].

Results and discussion

Our hypothesis on the reaction mechanism is illustrated in Scheme 3. In the chiral complexes **M3** and **M3'**, as shown in Scheme 4, carbonyl insertion has two possible pathways: C7 attacking C6 was denoted "**a**", while C7 attacking C1 was denoted "**b**". The relative free energies, ΔG(sol) including solvent energies, and the relative gas phase free energies, ΔG, enthalpies ΔH, and ZPE corrected electronic energies, ΔE, were relative to [$Mo(CO)_4$+R], and are summarized in Table S1. Unless otherwise noted, the energies discussed in the following are the relative free energies [ΔG(sol)].

The complexation reaction of 3-allyloxy-1-propynylphosphonates and $Mo(CO)_6$

The complexation reaction of $Mo(CO)_6$ with 3-allyloxy-1-propynylphosphonates (**R**) led to four possible complexes: **M1**, **M1'**, **M2**, and **M2'** (Fig. 1). The first two were formed through a π backdonation between molybdenum and a C–C double or triple bond, while the latter two were formed through two π backdonations between molybdenum and C–C double and triple bonds. The exchange of a CO ligand with an alkene or alkyne molecule (the double or triple bond of **R**) required about 73.8 or 82.5 kJ/mol, respectively. The exchange of two CO ligands with **R** required about 165.4 and 164.6 kJ/mol, forming **M2** and **M2'**. The barriers of 165.4 and 164.6 kJ/mol were too high to take place, which was consistent with the report of Imhof et al. [26].

The decomposition of two CO ligands from the catalyst $Mo(CO)_6$ resulted in the activated catalyst $Mo(CO)_4$, which coordinated with the reactant **R** to give the complexes **M2** and **M2'**. The formation of **M2** and **M2'** was exergonic, and the total free energies released were −124.0 and −124.8 kJ/mol, respectively. Obviously, the complexation reaction of the reactant with $Mo(CO)_4$ was easier than that with $Mo(CO)_6$. Therefore, in our hypothesis on the reaction mechanism (Scheme 3), the first step was the complexation reaction of $Mo(CO)_4$ with 3-allyloxy-1-propynylphosphonates (**R**), which agreed with the report of Imhof et al. [26]. It must be pointed out here that the transition states for the formation of the intermediates **M1**, **M1'**, **M2**, and **M2'** were not obtained by means of the optimization of structures.

The Mo-alkynyl-alkenyl complexes **M2** and **M2'** have similar geometry and energy. The difference is in the relative position of the alkenyl ligand relative to the other ligands. Atom C5 is sp^2-hybridized, and is a prochiral carbon, so **M2**

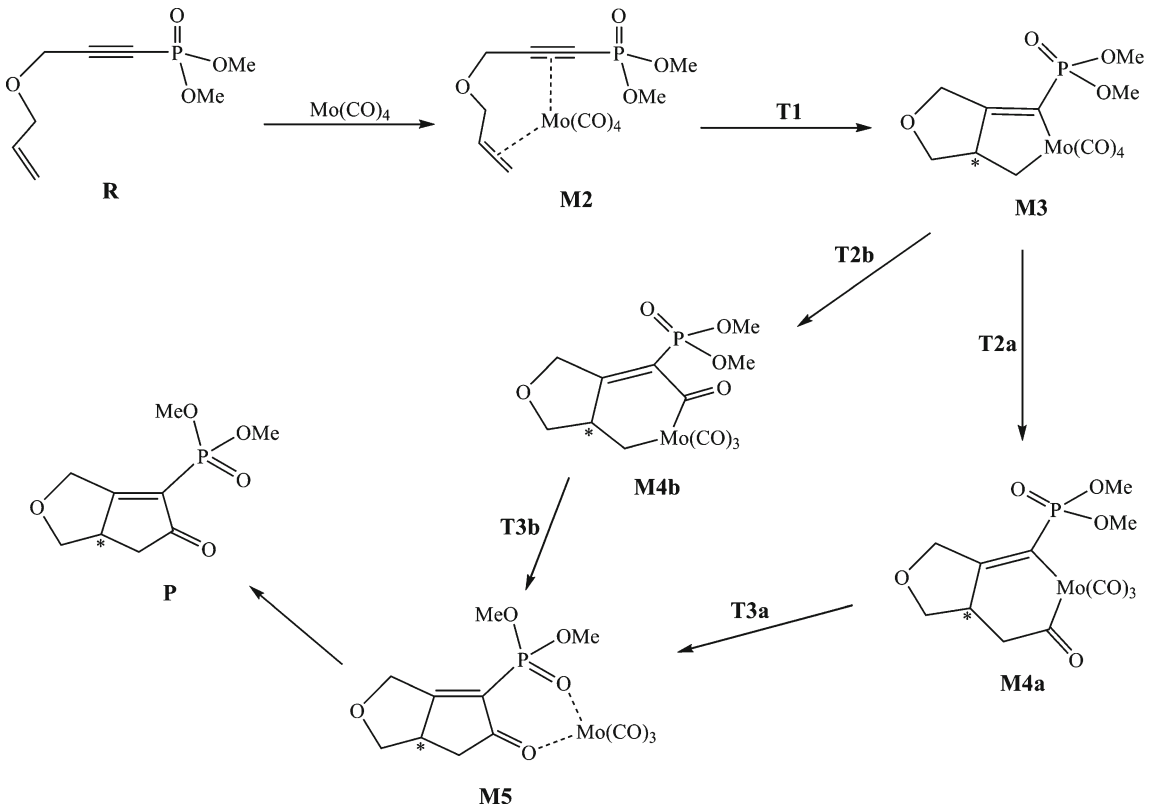

Scheme 3 Possible reaction mechanism of the Mo-catalyzed intramolecular PKR of substituted dimethyl 3-allyloxy-1-propynylphosphonates

Scheme 4 Two possible pathways of the carbonyl insertion reaction in complexes **M3** and **M3'**

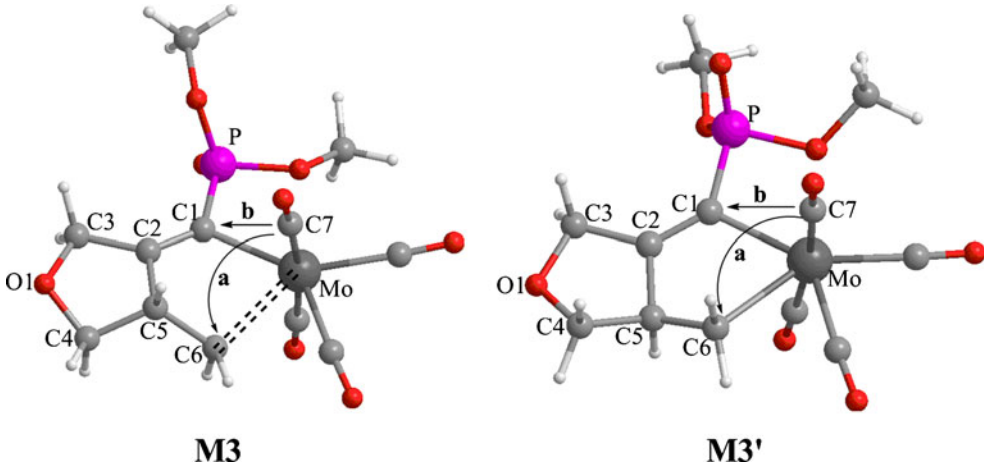

and **M2'** have a different prochiral surface. In **M2**, the lengths of the Mo–C1, Mo–C2, Mo–C5, and Mo–C6 bonds were 2.441, 2.486, 2.604, and 2.525 Å, respectively. In **M2'**, the lengths of the Mo–C1, Mo–C2, Mo–C5, and Mo–C6 bonds were, respectively, 2.371, 2.399, 2.680, and 2.558 Å. The C2-Mo-C5 angles were 68.7° for **M2** and 69.6° for

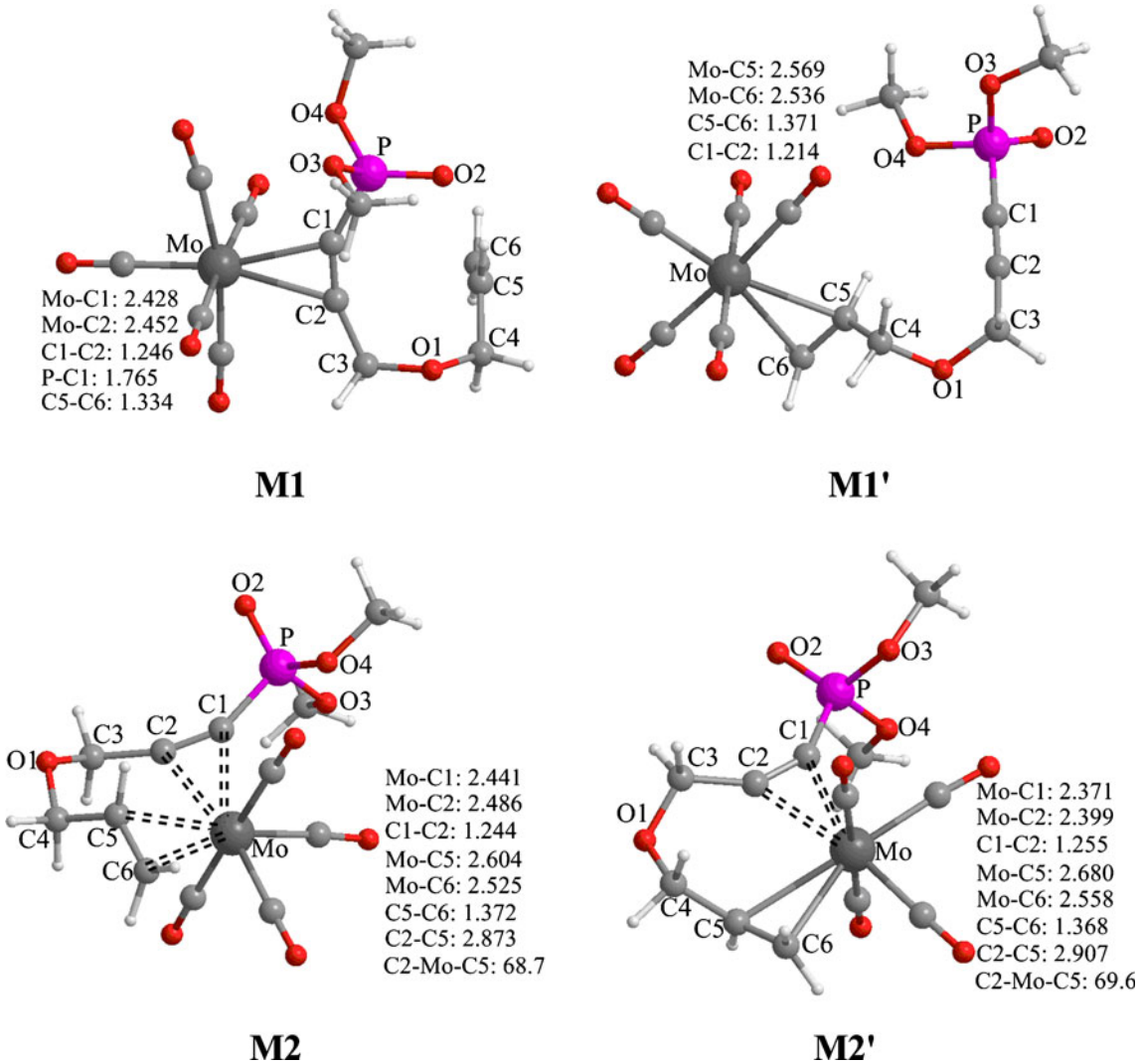

Fig. 1 Optimized structures of the $Mo(CO)_5$(**R**) complexes **M1** and **M1'**, and the $Mo(CO)_4$(**R**) complexes **M2** and **M2'** (selected bond lengths are given in Å, angles in degrees)

M2'. NBO analysis of **M2** and **M2'** showed there were two π backdonation bonds between molybdenum and π_{C1-C2} or π_{C5-C6} bond. The formation of the π backdonation weakened and activated the C1–C2 and C5–C6 bonds, which resulted in the attack of C2 on C5.

Formation of a product with (*S*)-chirality

Figure 2 shows the potential energy hypersurface for pathways forming the product with (*S*)-chirality **P**. The C–C oxidative cyclization transition state **T1** with Gibbs free energy of −77.1 kJ/mol leading to the complex **M3** was the chirality-determining step in the process of forming **P**. Next, intermediate **M3** underwent a carbonyl insertion through the transition states **T2a** and **T2b** with Gibbs free energies of −64.7 and −62.9 kJ/mol to give complexes **M4a** and **M4b**, respectively. Finally, intermediates **M4a** and **M4b** went through a reductive elimination reaction via transition states **T3a** and **T3b** with Gibbs free energies of −46.5 and −17.1 kJ/mol to form complex **M5**, which readily decomposed to yield the product of (*S*)-chirality **P**. Clearly, **T3a** and **T3b** were the highest stationary point in each reaction channel, so the reductive elimination reaction was the rate-determining step. Reaction pathway "**a**" was more favorable in the process of forming the product of (*S*)-chirality **P**. Therefore, the carbonyl insertion reaction into the Mo–C(sp^3) bond was easier than into the Mo–C=C bond in the process of forming **P**.

In $\sigma_{(C2-C5)}$ bond formation, the distances d_{C2-C5}, d_{Mo-C1}, and d_{Mo-C6} decreased, while d_{C1-C2} and d_{C5-C6} increased (Fig. 3). It was clear that a significant interaction between C2 and C5 occurred, and the C1–C2 and C5–C6 bonds were weakened considerably, as demonstrated by analyzing the changes in the bond orders, P_{ij}, and electron densities, ρ, at the BCPs (Table S3, e.g., C2–C5 bond, P_{ij}, **M2**: 0.000→**T1**: 0.528→**M3**: 0.864; ρ, **M2**: 0.000→**T1**: 0.104→**M3**: 0.265 e·Å^{-3}). As illustrated in Fig. 4, the HOMO for **T1** was a mixture of 47.4% HOFO-1, 26.0% HOFO-2 for $Mo(CO)_4$ (fragment 1) and 15.5% HOFO-1 for **R** (fragment 2). And LUMO was a mixture of 36.4% HOFO, 11.4% LUFO+7 for $Mo(CO)_4$ and 42.2% LUFO for **R**. Clearly, the reaction between $Mo(CO)_4$ and **R** occurred dominantly between HOFO-1, HOFO, and HOFO-2 of fragment 1 and LUFO and HOFO-1 of fragment 2. The net charge donation, which included both charge donation and electronic polarization contributions, was 0.05 of electrons. Hence, these facts suggested that, in the oxidative cyclization, $Mo(CO)_4$ donated electrons to **R**, which would result in the formation of the C2–C5, Mo–C1, and Mo–C6 bonds. The high stabilization energies of 483.8, 459.8, and 386.6 kJ/mol for the $\sigma_{Mo-C6}\rightarrow\sigma^*_{Mo-C(CO)}$, $\sigma_{Mo-C1}\rightarrow\sigma^*_{Mo-C(CO)}$, $\sigma_{Mo-C1}\rightarrow\sigma^*_{Mo-C6}$ in **T1** (Table 1), which was obtained from the second-order perturbation analysis of donor-acceptor interactions in the NBO analysis and used to estimate the strengths of the donor-acceptor interactions of the NBOs, revealed the strong interaction between σ_{Mo-C6} and $\sigma^*_{Mo-C(CO)}$, σ_{Mo-C1} and $\sigma^*_{Mo-C(CO)}$, σ_{Mo-C1} and σ^*_{Mo-C6}, and the electron transfer tendency from σ_{Mo-C6} to $\sigma^*_{Mo-C(CO)}$, σ_{Mo-C1} to $\sigma^*_{Mo-C(CO)}$, σ_{Mo-C1} to σ^*_{Mo-C6}. NBO analysis also indicated that the Mo–C1 and Mo–C6 bonds showed a strong single-bonded character, and the NBO energies of the bonding orbitals σ_{Mo-C1} and σ_{Mo-C6} were −617 and −500 kJ/mol, respectively. In **M3**, Mo–C1, Mo–C6, and Mo–O3 bonds were 2.203, 2.462, 2.417 Å, respectively. Obviously, a significant interaction between Mo and O3 occurred, with a group methoxy of phosphonate coordinating to molybdenum. NBO analysis of **M3** indicated that the Mo–C1 and Mo–C6 bonds showed a strong single-bonded character, so the π back-donation between molybdenum and π_{C1-C2} or

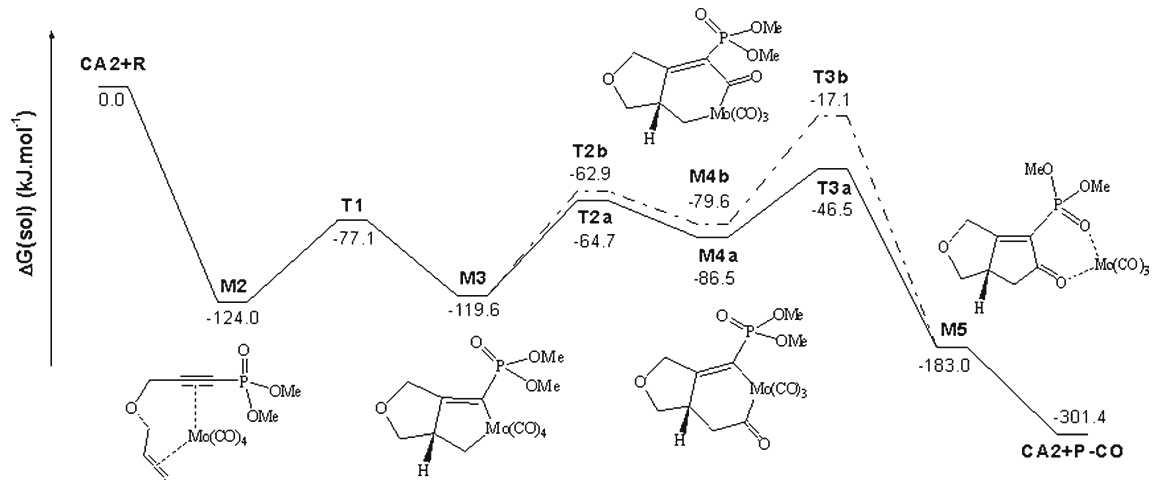

Fig. 2 Free energy profiles for the proposed pathways forming the product of (*S*)-chirality **P**

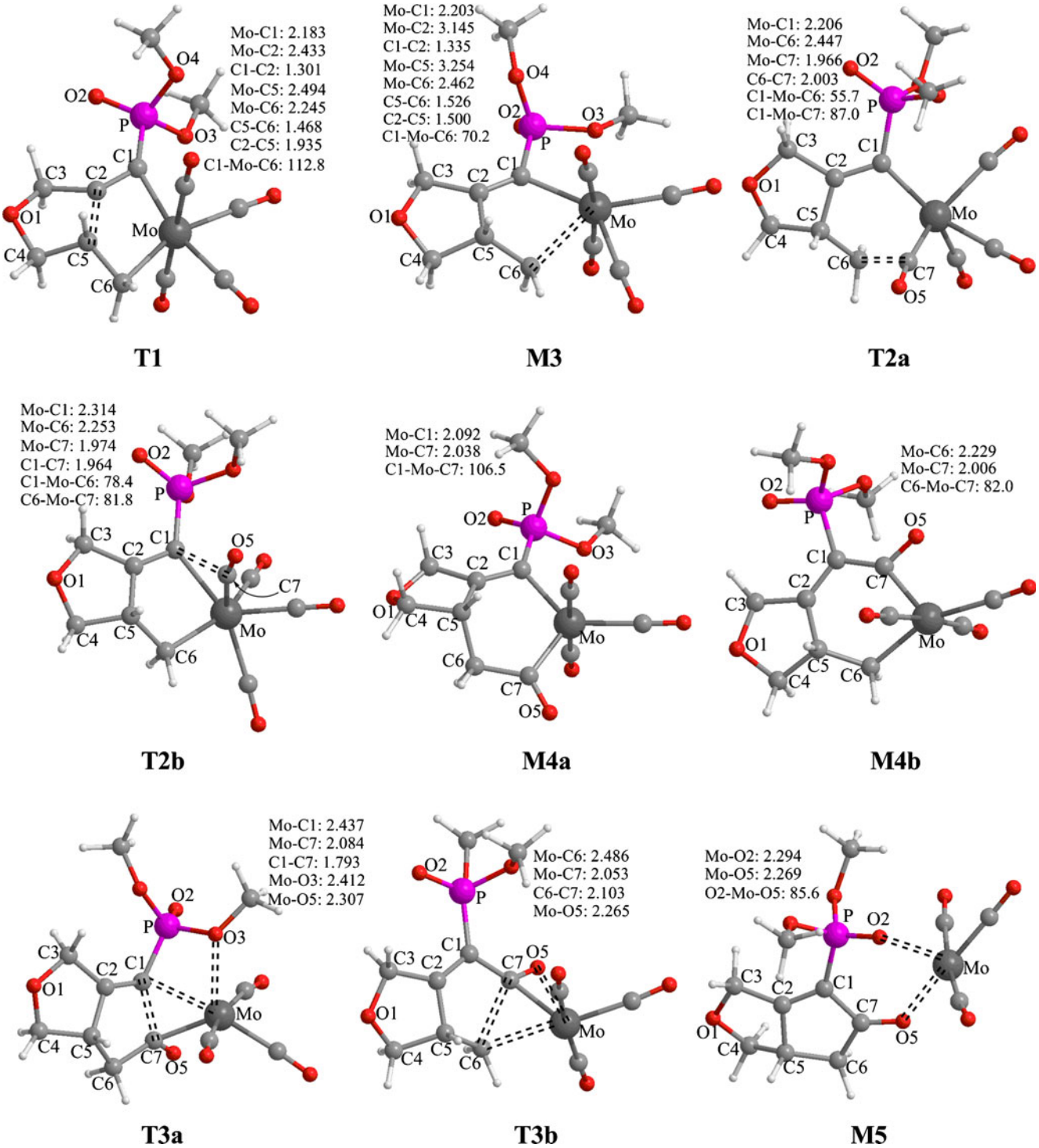

Fig. 3 Intermediates and transition states of the formation of the product of (*S*)-chirality in the Mo-catalyzed intramolecular Pauson-Khand reaction (PKR) (selected bond lengths are given in Å, angles in degrees)

π_{C5-C6} bond was disrupted. The atom C5 was sp^3-hybridized, and was of (*S*)-chirality. There was one Mo–C1–C2–C5–C6 five-membered ring, and the electron density of the RCP was 0.03 e·Å^{-3}.

The carbonyl insertion had two possible reaction pathways. **T2a** and **M4a** involved a Mo–C1–C2–C5–C6–C7 six-membered ring, and the electron densities of the RCPs were 0.02 and 0.02 e·Å^{-3}, respectively. NBO analysis of **M4a** indicated that the Mo–C1 and Mo–C7 bonds showed a strong single-bonded character, and NBO energies were −1,053 and −1,140 kJ/mol, respectively. **T2b** and **M4b** involved a Mo–C7–C1–

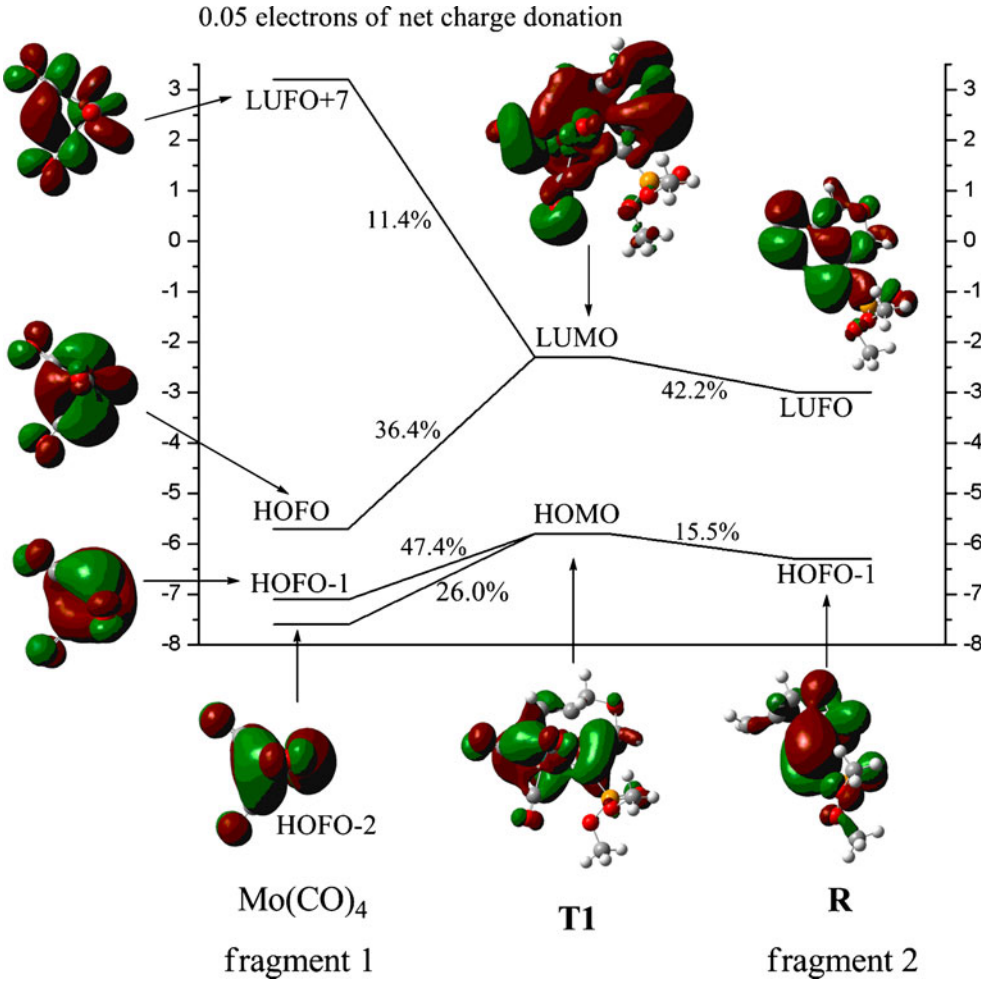

Fig. 4 Orbital interaction diagram for **T1**, which was formed by $Mo(CO)_4$ and 3-allyloxy-1-propynylphosphonates (**R**). The AOMix-CDA calculation, based on the B3LYP/6-31 G(d,p) results [LANL2DZ(f) for Mo]. The net charge donation CT(1→2) − CT (2→1) was 0.05 electrons

C2–C5–C6 six-membered ring, and the electron densities of the RCPs were 0.02 and 0.02 e·Å^{-3}, respectively. The Mo–C6 and Mo–C7 bonds of **M4b** showed strong single-bonded character.

T3a and **T3b** were the transition states of the reductive elimination reaction, and involved a C1–C2–C5–C6–C7 five-membered ring; the electron densities of the RCPs were 0.03 and 0.03 e·Å^{-3}, respectively. The Gibbs free energy of

Table 1 Selected stabilization interaction energies E(2) for **T1** and **T3a** (kJ/mol)

T1		**T3a**	
Donor NBO→acceptor NBO	*E(2)*	Donor NBO→acceptor NBO	*E(2)*
BD Mo-C(CO)→BD* Mo-C6	232.6	BD C1-C7→BD* Mo-C(CO)	169.3
BD Mo-C(CO)→BD* Mo-C1	274.4	BD C1-C7→BD* C2-C3	38.0
BD Mo-C6→BD* Mo-C(CO)	483.8	BD C1-P→BD* Mo-C(CO)	65.8
BD Mo-C6→BD* Mo-C1	274.5	BD C1-P→BD* C2-C3	13.7
BD Mo-C1→BD* Mo-C(CO)	459.8	BD C1-P→BD* C2-C5	15.4
BD Mo-C1→BD* Mo-C6	386.6	LP(2) O3→LP*(2) Mo	117.8
BD C1-C2→BD* Mo-C(CO)	73.4	LP(2) O5→BD* C1-C7	172.0
π C1-C2→BD* Mo-C(CO)	55.2	LP(3) O5→BD* Mo-C7	418.0
BD C2-C5→BD* Mo-C(CO)	133.0		
BD C2-C5→BD* Mo-C1	28.8		
BD C2-C5→BD* Mo-C6	46.9		
BD C5-C6→BD* Mo-C(CO)	97.9		

T3a was lower than **T3b** by 29.4 kJ/mol, due to the formation of a coordinate bond between Mo and O3 in **T3a** (2.412 Å). As summarized in Table 1, the high stabilization energies of 418.0, 172.0, 169.3, and 117.8 kJ/mol for $(2p)_{O5} \rightarrow \sigma^*_{Mo-C7}$, $(2\ s)_{O5} \rightarrow \sigma^*_{C1-C7}$, $\sigma_{C1-C7} \rightarrow \sigma^*_{Mo-C(CO)}$, $(2\ s)_{O3} \rightarrow (4\ d)^*_{Mo}$ in **T3a** revealed the strong interaction between $(2p)_{O5}$ and σ^*_{Mo-C7}, $(2\ s)_{O5}$ and σ^*_{C1-C7}, σ_{C1-C7} and $\sigma^*_{Mo-C(CO)}$, $(2\ s)_{O3}$ and $(4\ d)^*_{Mo}$, and the electron transfer tendency from $(2p)_{O5}$ to σ^*_{Mo-C7}, $(2\ s)_{O5}$ to σ^*_{C1-C7}, σ_{C1-C7} to $\sigma^*_{Mo-C(CO)}$, $(2\ s)_{O3}$ to $(4\ d)^*_{Mo}$. Hence, the interaction between molybdenum and two oxygen atoms O3 and O5 made **T3a** more stable. The atomic polar tensor (APT) charges of carbon atoms of C1–C7 bond are −0.786 and +1.166.

Formation of a product of (*R*)-chirality

Figure 5 shows the potential energy hypersurface of the pathways forming the product of (*R*)-chirality **P'**. The C–C oxidative cyclization transition state **T1'** with Gibbs free energy of −76.6 kJ/mol leading to complex **M3'** was again the chirality-determining step in the process of forming **P'**. Intermediate **M3'** then underwent a carbonyl insertion through the transition states **T2a'** and **T2b'** with the Gibbs free energies of −56.7 and −24.9 kJ/mol to form the complexes **M4a'** and **M4b'**, respectively. Finally, intermediates **M4a'** and **M4b'** went through the reductive elimination reaction via the transition states **T3a'** and **T3b'** with the Gibbs free energies of −19.6 and −40.2 kJ/mol to generate the complex **M5'** releasing the product of (*R*)-chirality **P'**. In the reaction pathway "**a**", the reductive elimination reaction was the rate-determining step, while the carbonyl insertion was the rate-determining step in reaction pathway "**b**". (These results were not in agreement with those discussed above in the process of forming **P**.) Evidently, reaction pathway "**b**" was more favorable in the process of forming the product of (*R*)-chirality **P'**. So the carbonyl insertion reaction into the Mo-C(sp^3) bond was more difficult than into the Mo–C=C bond in the process of forming **P'**, which was different from those discussed above in the process of forming **P**.

In $\sigma_{(C2-C5)}$ bond formation, as illustrated in Fig. 6, the distances d_{C2-C5}, d_{Mo-C1}, and d_{Mo-C6} decreased, while d_{C1-C2} and d_{C5-C6} increased. It was clear that a significant interaction between C2 and C5 occurred, and the C1–C2 and C5–C6 bonds were weakened considerably. NBO analysis of **M3'** indicated that the Mo–C1 and Mo–C6 bonds showed strong single-bonded character, so the π backdonation between molybdenum and π_{C1-C2} or π_{C5-C6} bond was disrupted. Atom C5 was sp^3-hybridized, and was of (*R*)-chirality, which was different from **M3**. **T2a'** and **T2b'** were the transition states of the carbonyl insertion, and involved a Mo–C1–C2–C5–C6–C7 or Mo–C7–C1–C2–C5–C6 six-membered ring. **T3a'** and **T3b'** were the transition state of the reductive elimination reaction, and involved a C1–C2–C5–C6–C7 five-membered ring.

Overview of the reaction mechanism

As discussed above, the dominant reaction pathways were outlined in Scheme 3. The calculated results indicate that the Mo-catalyzed intramolecular PKR of 3-allyloxy-1-propynylphosphonates was exergonic, and that the total free energy released was −301.4 kJ/mol. The C–C oxidative cyclization reaction was the chirality-determining step.

In the process of forming the product of (*S*)-chirality **P**, the reductive elimination reaction was the rate-determining step, and reaction pathway "**a**" was more favorable (i.e.. the carbonyl insertion reaction into the Mo-C(sp^3) bond was easier than into the Mo-C=C bond.). The reaction pathway

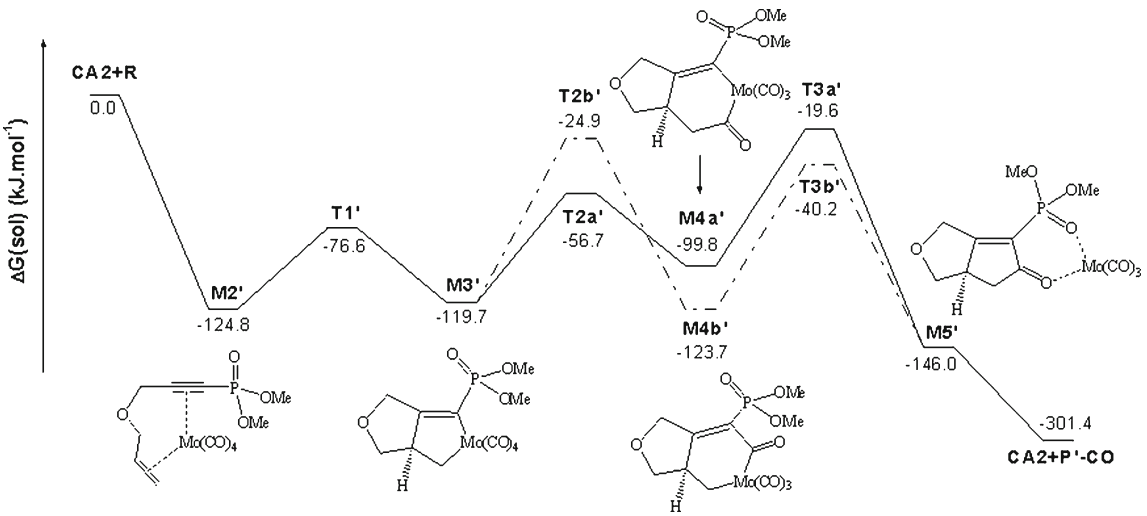

Fig. 5 Free energy profiles for the proposed pathways forming the product of (*R*)-chirality **P'**

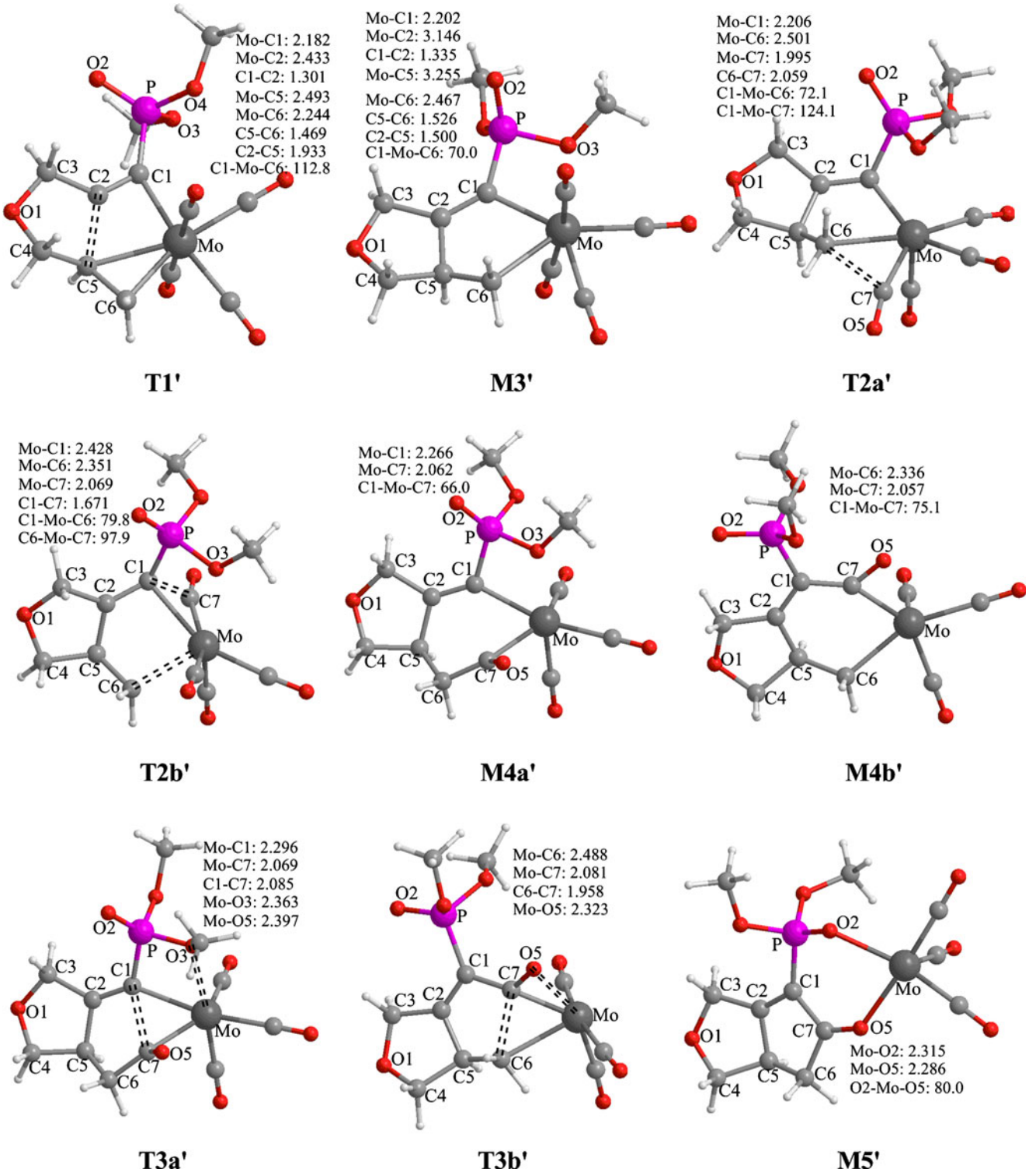

Fig. 6 Intermediates and transition states of the formation of the product of (*R*)-chirality in the Mo-catalyzed intramolecular PKR (selected bond lengths are given in Å, angles in degrees)

CA2+R→M2→T1→M3→T2a→M4a→T3a→M5→P was more favorable. Thus, in the process of forming the product of (*R*)-chirality **P'**, the reductive elimination reaction was the rate-determining step for reaction pathway "**a**", while the carbonyl insertion was the rate-determining step for reaction pathway "**b**". Reaction pathway "**b**" was more favorable, so the carbonyl insertion reaction into the Mo–C(sp^3) bond was more difficult than into the Mo–C=C

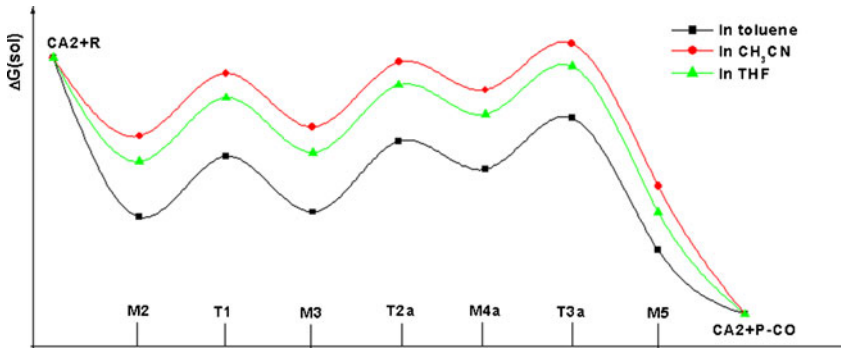

Fig. 7 Free energy profiles of the most favorable pathway in the three solvents toluene, CH_3CN, and THF

bond. The reaction pathway **CA2+R→M2'→T1'→M3'→T2b'→M4b'→T3b'→M5'→P'** was more favorable.

Because the Gibbs free energy of **T3a** was lower by 21.6 kJ/mol than **T2b'**, the reaction pathway "**a**" forming **P** was more dominant. Therefore, the reaction pathway **CA2+R→M2→T1→M3→T2a→M4a→T3a→M5→P** was the most favorable in the Mo-catalyzed intramolecular PKR, and the dominant product predicted theoretically was of (*S*)-chirality, which was consistent with experiments [25].

Effects of the solvent

Srebnik et al. [25] also proved that the intramolecular PKR was solvent dependent. The highest yield was obtained in toluene with a temperature of 373.15 K, with much lower yields being obtained in CH_3CN or THF at temperatures of 355.15 or 333.15 K, respectively.

To evaluate the solvent effect of toluene (ε=2.379), CH_3CN (ε=36.64), and THF (ε=7.58), single-point computations were performed at the B3LYP/6-31 G(d,p) level [LANL2DZ (f) for Mo] using the PCM model with the default parameters, except for the temperature (373.15 K for toluene, 355.15 K for CH_3CN, and 333.15 K for THF were used) [25]. The relative free energies, ΔG(sol) including solvent energies, of all species in the three solvents are summarized in Table S2.

As shown in Table S2, in the three solvents toluene, CH_3CN, and THF, the dominant reaction pathway was consistent, and the rate-determining step was the reductive elimination reaction. The effect of the three solvents on the most favorable pathway is illustrated in Fig. 7: the black line shows the free energy profile in toluene; the red line shows the free energy profile in CH_3CN; the green line shows the free energy profile in THF. Evidently, the free energies of the stationary points of the most favorable pathway in toluene were lower than those in CH_3CN or THF. The free energies of the transition states of the rate-determining step in toluene, CH_3CN, and THF were −46.5, 11.2, and −6.1 kJ/mol, respectively. Therefore, we conclude that the reaction is solvent dependent, with toluene being the best among the three solvents.

As shown in Table S1, the solvation effect was considerable. It decreased the free energies of all intermediates and transition states.

Conclusions

The reaction mechanisms of the Mo-catalyzed intramolecular PKR of 3-allyloxy-1-propynylphosphonates were explored computationally using DFT [at the B3LYP/6-31 G(d,p) level; LANL2DZ(f) for Mo]. The calculated results indicate that the $Mo(CO)_6$-catalyzed intramolecular Pauson-Khand reaction is exergonic, and that the total free energy released was −301.4 kJ/mol.

The reaction pathway **CA2+R→M2→T1→M3→T2a→M4a→T3a→M5→P** was the most favorable among all of the reaction channels of the Mo-catalyzed intramolecular PKR. The reductive elimination reaction was the rate-determining step for this pathway, and the dominant product predicted theoretically was of (*S*)-chirality. The C–C oxidative cyclization reaction was the chirality-determining step. The carbonyl insertion reaction into the Mo–C(sp^3) bond was easier than into the Mo–C=C bond.

This reaction was solvent dependent, and toluene was a better solvent than CH_3CN and THF. The solvation effect was considerable. It decreased the free energies of all intermediates and transition states.

Acknowledgments This work was supported by the Key Project of Science and Technology of the Ministry of Education, P. R. (grant No. 104263), Natural Science Foundation of Chongqing City, P. R. (grant No. CSTC-2004BA4024).

Supporting information All energies, Wiberg bond orders P_{ij} and electron density ρ (e·Å^{-3}) at BCPs of some selected bonds are given by the supporting information.

References

1. Khand IU, Knox GR, Pauson PL, Watts WE, Foreman MI (1973) J Chem Soc Perkin Trans 1:975–977

2. Khand IU, Knox GR, Pauson PL, Watts WE, Foreman MI (1973) J Chem Soc Perkin Trans 1:977–981
3. Pauson PL, Khand IU, Ann NY (1977) Acad Sci 295:2–14
4. Pauson PL (1985) Tetrahedron 41:5855–5860
5. Murakami M, Amii H, Ito Y (1994) Nature 370:540–541
6. Blance-Urgoito J, Anorbe L, Pérez-Senano L, Domingcez G, Pérez-Castells J (2004) Chem Soc Rev 33:32–42
7. Brummond KM, Kent JL (2000) Tetrahedron 56:3263–3283
8. Chung YK (1999) Coord Chem Rev 188:297–341
9. Strübing D, Beller M (2006) Top Organomet Chem 18:165–178
10. Shibata T (2006) Adv Syn Catal 348:2328–2336
11. Shibata T, Toshida N, Takagi K (2002) Org Lett 4:1619–1621
12. Shibata T, Toshida N, Takagi K (2002) J Org Chem 68:7446–7450
13. Morimoto T, Fuji K, Tsutsumi K, Kakiuchi K (2002) J Am Chem Soc 124:3806–3807
14. Fuji K, Morimoto T, Tsutsumi K, Kakiuchi K (2003) Angew Chem Int Ed 42:2409–2411
15. Morimoto T, Kakiuchi K (2004) Angew Chem Int Ed 43:5580–5588
16. Kwong FY, Lee HW, Qiu L, Lam WH, Li YM, Kwong HL, Chan ASC (2005) Adv Syn Catal 347:1750–1754
17. Kent JL, Wan H, Brummond KM (1995) Tetrahedron Lett 36:2407–2410
18. Minami T, Okauchi T, Kouno R (2001) Synthesis 349–357
19. Dembitsky VM, Al Quntar AAA, Haj-Yehia A, Srebnik M (2005) MiniRev Org Chem 2:91–109
20. Maffei M (2004) Curr Org Synth 1:355–375
21. Quntar AA, Baum O, Reich R, Srebnik M (2004) Arch Pharm 337:76–80
22. Quntar AA, Gallily R, Katzavian G, Srebnik M (2007) Eur J Pharmacol 556:9–13
23. Cristau HJ, Gasc MB, Mbianda XY, Geze A (1996) Phosphorus Sulfur Silicon Relat Elem 111:159–159
24. Rivero MR, Carretero JC (2003) J Org Chem 68:2975–2978
25. Moradov D, Quntar AAAA, Youssef M, Smoum R, Rubinstein A, Srebrnik M (2009) J Org Chem 74:1029–1033
26. Imhof W, Anders E, Göbel A, Görls H (2003) Chem Eur J 9:1166–1181
27. Fjermestad T, Pericàs MA, Maseras F (2011) Chem Eur J 17:10050–10057
28. Wang C, Wu YD (2007) Organometallics 27:6152–6162
29. Baik MH, Mazumder S, Ricci P, Sawyer JR, Song YG, Wang H, Evans PA (2008) J Am Chem Soc 133:7621–7623
30. Baik MH, Mazumder S, Ricci P, Sawyer JR, Song YG, Wang H, Evans PA (2011) J Am Chem Soc 130:5821–5830
31. Gimbert Y, Lesage D, Milet A, Fournier F, Greene AE, Tabet JC (2003) Org Lett 5:4073–4075
32. Frisch MJ, Trucks GW, Schlegel HB, Scuseria GE, Robb MA, Cheeseman JR, Montgomery JA, Vreven JT, Kudin KN, Burant JC, Millam JM, Iyengar SS, Tomasi J, Barone V, Mennucci B, Cossi M, Scalmani G, Rega N, Petersson GA, Nakatsuji H, Hada M, Ehara M, Toyota K, Fukuda R, Hasegawa J, Ishida M, Nakajima T, Honda Y, Kitao O, Nakai H, Klene M, Li X, Knox JE, Hratchian HP, Cross JB, Adamo C, Jaramillo J, Gomperts R, Stratmann RE, Yazyev O, Austin AJ, Cammi R, Pomelli C, Ochterski JW, Ayala PW, Morokuma K, Voth GA, Salvador P, Dannenberg JJ, Zakrzewski VG, Dapprich S, Daniels AD, Strain MC, Farkas O, Malick DK, Rabuck AD, Raghavachari K, Foresman JB, Ortiz JV, Cui Q, Baboul AG, Clifford S, Cioslowski J, Stefanov BB, Liu G, Liashenko A, Piskorz P, Komaromi I, Martin RL, Fox DJ, Keith T, Al-Laham MA, Peng CY, Nanayakkara A, Challacombe M, Gill PMW, Johnson B, Chen W, Wong MW, Gonzalez C, Pople JA (2004) Gaussian 03, Revision B.05. Gaussian Inc, Pittsburgh PA
33. Parr RG, Yang W (1989) Density-functional theory of atoms and molecules. Oxford University Press, New York
34. Becke AD (1993) J Chem Phys 98:5648–5652
35. Lee C, Yang W, Parr RG (1988) Phys Rev B 37:785–789
36. Hay PJ, Wadt WR (1985) J Chem Phys 82:270–283
37. Wadt WR, Hay PJ (1985) J Chem Phys 82:284–297
38. Hay PJ, Wadt WR (1985) J Chem Phys 82:299–310
39. Ehlers AW, Böhme M, Dapprich S, Gobbi A, Höllwarth A, Jonas V, Köhler KF, Stegmann R, Veldkamp A, Frenking G (1993) Chem Phys Lett 208:111–114
40. Gonzalez C, Schlegel HB (1990) J Phys Chem 94:5523–5527
41. Flükiger P, Lüthi HP, Portmann S, Weber J (2000–2002) MOLEKEL 4.3 Swiss Center for Scientific Computing, Manno. Switzerland
42. Portmann S, Lüthi HP (2000) Chimia 54:766–770
43. Carpenter JE, Weinhold F (1988) J Mol Struct THEOCHEM 169:41–50
44. Foster JP, Weinhold F (1980) J Am Chem Soc 102:7211–7218
45. Reed AE, Weinstock RB, Weinhold F (1985) J Chem Phys 83:735–746
46. Reed AE, Curtiss LA, Weinhold F (1988) Chem Rev 88:899–926
47. Glendening ED, Badenhoop JK, Reed AE, Carpenter JE, Bohmann JA, Morales CM, Weinhold F (2001) NBO 5.0, Theoretical Chemistry Institute, University of Wisconsin, Madison, WI
48. Marten B, Kim K, Cortis C, Friesner RA, Murphy RB, Ringnalda MN, Sitkoff D, Honig B (1996) J Phys Chem 100:11775–11788
49. Friesner RA, Murphy RB, Beachy MD, Ringnalda MN, Pollard WT, Dunietz BD, Cao YX (1999) J Phys Chem A 103:1913–1928
50. Miertus S, Tomasi J (1982) Chem Phys 65:239–245
51. Gorelsky SI, Lever ABP (2001) J Organomet Chem 635:187–196
52. Gorelsky SI (1997) AOMix: program for molecular orbital analysis. York University, Toronto, Canada; http://www.sf-chem.net/
53. Gorelsky SI, Ghosh S, Solomon EI (2006) J Am Chem Soc 128:278–290
54. Bader RFW (1990) Atoms in molecules, a quantum theory; International series of monographs in chemistry, vol 22. Oxford University Press, Oxford, UK
55. Biegler-König F, Schönbohm J, Derdau R, Bayles D, Bader RFW (2002) AIM 2000. Version 2.0, McMaster University